Inorganic Chemistry 56.19 (2017): 11810-11818
DOI: https://doi.org/10.1021/acs.inorgchem.7b01775

SUPPORTING INFORMATION

Group 10 metal benzene-1,2-dithiolate derivatives in synthesis of coordination polymers containing potassium countercations

Oscar Castillo,[a] Esther Delgado,[b] Carlos J. Gómez-García,[c] Diego Hernández,[b] Elisa Hernández,[b] Avelino Martín,[d] José I. Martínez[e] and Félix Zamora[b,f]**

[a]Departamento de Química Inorgánica, Universidad del País Vasco. Apartado 644, e–48080 Bilbao, Spain. [b]Departamento de Química Inorgánica, Universidad Autónoma de Madrid, 28049 Madrid, Spain. [c]Instituto de Ciencia Molecular. Universidad de Valencia. C/ Catedrático José Beltrán, 2. 46980 Paterna, Valencia, Spain. [d]Departamento de Química Inorgánica, Universidad de Alcalá. Campus Universitario, E-28871, Alcalá de Henares, Spain. [e]Departamento de Nanoestructuras, Superficies, Recubrimientos y Astrofísica Molecular. Instituto de Ciencia de Materiales de Madrid (ICMM-CSIC), 28049 Madrid, Spain. [f]Institute for Advanced Research in Chemical Sciences (IAdChem). Universidad Autónoma de Madrid, 28049 Madrid, Spain.

S1. Theoretical Studies

It is interesting to notice the important differences observed in the packing models between the building blocks for the different $[M(SC_6H_4S)_2]$ and $[M(SC_6H_2Cl_2S)_2]$-based Ni, Pd and Pt crystals. Meanwhile for the $[Ni(SC_6H_4S)_2]$ and $[Pd(SC_6H_4S)_2]$-based compounds the two K atoms per unit cell are located: i) one of them on a C-ring hollow site (mostly interacting with the inner C-C bridge close to the S atoms), and ii) the other one on a S-S bridge, for the $[Pt(SC_6H_4S)_2]$-based compound both K atoms are located on each available S-S bridges. On the other hand, within the $[M(SC_6H_2Cl_2S)_2]$-based Ni, Pd and Pt crystals the interaction of the two K atoms per unit cell is always produced with the Cl and S atoms. In order to rationalize these different packing behaviors within each crystal we have carried out a set of first-principles DFT-based calculations. For that purpose we have made use of the concept of the Fukui functions $f^{\pm}(\boldsymbol{r})$[6,7] defined as:

$$f^{\pm}(\boldsymbol{r}) = \left[\frac{\partial \rho(\boldsymbol{r})}{\partial N}\right]^{\pm}_{v}, \qquad (1)$$

which measure the change in the chemical potential as the number of electrons changes from N to $N+dN$ or to N-dN, respectively. In particular, given that the $[M(SC_6H_4S)_2]$ and $[M(SC_6H_2Cl_2S)_2]$ units will act with a net charge state of -2 within each crystal, we have used the positive Fukui function $f^{+}(\boldsymbol{r})$ to elucidate sites with enhanced reactivity within the complexes $[M(SC_6H_4S)_2]$ and $[M(SC_6H_2Cl_2S)_2]$ for M=Ni, Pd and Pt as they accommodate extra electronic charge. By construction, $f^{+}(\boldsymbol{r})$ describes the way in which the electron density $\rho(\boldsymbol{r})$ changes as the number of electrons in the complex increases from N to $N+dN$ (in this case from 0 for the neutral case towards the accommodation of 2 extra electrons) at constant external potential.[6,7] This means that regions where $f^{+}(\boldsymbol{r})$ is large are able to stabilize an uptake electronic charge, and are reactive towards the anchoring electron-rich reactants nucleophiles. In practice, the two Fukui functions can be obtained using a finite difference approximation, as the density differences.[6,7]

$$\begin{aligned} f^{+}(\mathbf{r}) &= r_{v,N+1}(\mathbf{r}) - r_{v,N}(\mathbf{r}), \\ f^{-}(\mathbf{r}) &= r_{v,N}(\mathbf{r}) - r_{v,N-1}(\mathbf{r}) \end{aligned} \qquad (2)$$

We have computed the positive Fukui function $f^{+}(\boldsymbol{r})$ for the different isolated complexes $[M(SC_6H_4S)_2]$ and $[M(SC_6H_2Cl_2S)_2]$ with M=Ni, Pd and Pt (see Figures 1 and S1, respectively) based on the electronic charge densities obtained by the GAUSSIAN09 simulation package[8] within a quantum-chemistry all-electron B3LYP model accounting

for cc-pVQZ basis sets for H, C, S and Cl, and LanL2DZ basis sets for M=Ni, Pd and Pt (see details in Ref. 8). In all the calculations the most stable electronic spin-configuration is the low-spin (LS) state, in which all eight *d* electrons in the metal atom are paired (S=0). This is consistent with the well-known 4-coordinate [Ni(II)/Pd(II)/Pt(II)]S_4 square planar complexes,[9] just the present case in both the [$M(SC_6H_4S)_2$] and [$M(SC_6H_2Cl_2S)_2$] configurations.

In the Figure S1 we show the 3D isosurfaces corresponding to the Fukui function $f^+(\boldsymbol{r})$ for the different [$M(SC_6H_2Cl_2S)_2$] complexes (all with a value of +0.0005 e^- $Å^{-3}$). For all these three cases (M=Ni, Pd and Pt) we can observe that the function $f^+(\boldsymbol{r})$ adopts its highest values around the Cl and S atoms. Those regions will favor the stabilization and accommodation of extra electronic charge, being reactive towards the anchoring electron-rich reactants nucleophiles. This translates in that the preferential donor sites will be located at the S and Cl atoms, while the C-rings are almost deactivated therefore hampering any metal coordination. This is in agreement with our reported experimental observations.

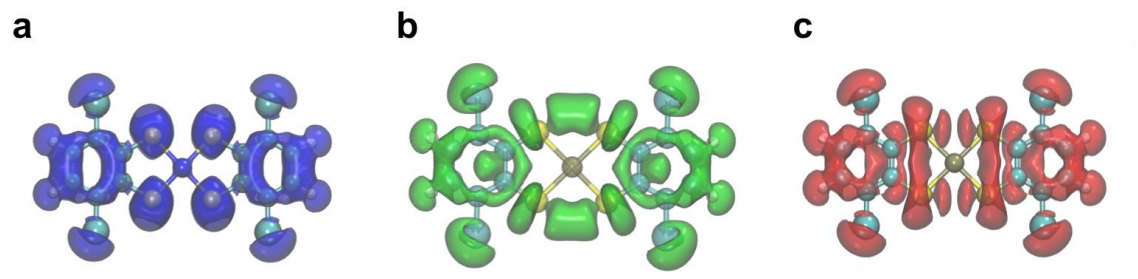

Figure S1. Computed 3D isosurfaces corresponding to the positive Fukui function $f^+(\boldsymbol{r})$ for the different isolated complexes [$M(SC_6H_2Cl_2S)_2$] for: a) M= Ni, b) M= Pd, and c) M= Pt. All the 3D isosurfaces are shown for a value of +0.0005 e^- $Å^{-3}$.

On the other hand, in the Figure 1 and Figure S2 we show the 3D isosurfaces corresponding to the Fukui function $f^+(\boldsymbol{r})$ for the different [$M(SC_6H_4S)_2$] (being M=Ni, Pd and Pt) complexes (all with a value of +0.0005 e^- $Å^{-3}$). Contrarily to the previous [$M(SC_6H_2Cl_2S)_2$] case, according to the results of the calculations in Figure 1 the most favorable options to accommodate the excess of electronic charge and anchor the two K atoms within the [$Ni(SC_6H_4S)_2$] and [$Pd(SC_6H_4S)_2$] units are on the C-rings (close to the inner C-C bond) and on a S-S bridge, being consistent with the K-K distances within each

crystal (indicated by black circles superimposed in the Figure 1). At this point, it is important to remark that in these two [Ni($SC_6H_4S)_2$] and [Pd($SC_6H_4S)_2$] latest cases the Fukui function $f^+(\boldsymbol{r})$ adopts large values simultaneously by symmetry in both S-S bridges with the possibility of linking the K atoms on them; nevertheless, given the equilibrium K-K distance within the crystals, the K atoms would not fit in this symmetric configuration: with a K-K distance too short for the case of the Ni compound, and too large for the Pd compound. On the contrary, for the case of [Pt($SC_6H_4S)_2$], the most favorable configuration arises from accommodating both K atoms on the two S-S bridges, which is indeed consistent with the K-K distance in this case. These findings are in excellent agreement with the experimental crystal configurations observed.

Summarizing, we herein demonstrate that the use of the Fukui function $f^+(\boldsymbol{r})$ to analyze the behavior of the different [M($SC_6H_4S)_2$] and [M($SC_6H_2Cl_2S)_2$] units towards the accommodation of extra charge can be used to rationalize their most reactive donor sites to anchor/link electron-rich reactants nucleophiles. This analysis can also offer interesting clues about how these complexes may pack when they are involved in the formation of complex crystals with other reactants, which turns this theoretical strategy into a powerful tool to elucidate in-silico crystal morphologies with a high degree of predictability.

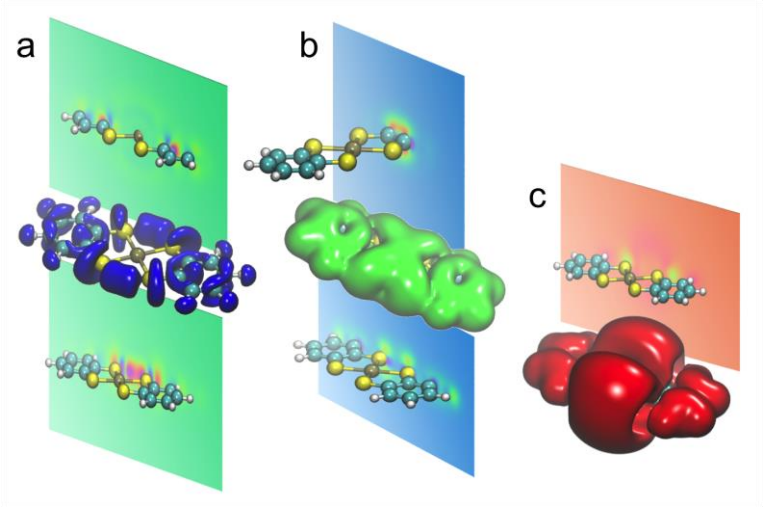

Figure S2. Computed 3D isosurfaces corresponding to the positive Fukui function f+(r) for the different isolated $[M(SC_6H_4S)_2]^{2-}$ entities [a) M = Ni, b) M = Pd, and c) M = Pt].The 3D isosurfaces are shown for isovalues of +0.0005 +0.0002 and +0.0001 $e^-Å^{-3}$, respectively in a), b) and c). Additionally, 2D color maps of the 3D isosurfaces corresponding to slices cutting the regions with a higher f+(r) spatial density are also shown in each panel.

Additionally, to further justify this interesting behavior, we have performed DFT-based calculations on the different building blocks (including the k-based ligands) in two different configurations each: a) in the configuration where the two K atoms per unit cell are located one of them on a C-ring hollow site (mostly interacting with the inner C-C bridge close to the S atoms) and the other one on a S-S bridge of the [$M(SC_6H_4S)_2$] units; and b) in the configuration where both K atoms are located on each S-S available bridges (Figure S3). For those configurations not experimentally evidenced – e.g., the Ni (a) and Pd (b) cases in configuration b); and the Pt (c) case in configuration a) – we have performed full geometrical optimization to minimize the net forces acting on each atom (below 0.1 eV $Å^{-1}$). These calculations have been carried out by the efficient plane-wave code QUANTUM ESPRESSO.[10] The exchange-correlation (XC) effects have been accounted for by using the revised version of the generalized gradient corrected approximation (GGA) of Perdew, Burke, and Ernzerhof (rPBE),[11] and RRKJ norm-conserving scalar-relativistic pseudopotentials have been considered to model the ion-electron interaction.[12] In these calculations, the Brillouin zones (BZ) were sampled by means of optimal Monkhorst-Pack grids[13] guaranteeing a full convergence in energy and electronic density. A perturbative van der Waals (vdW) correction was used to account long-range interaction and checking the reliability of all the structures.[14,15]

The result of the calculations reveal that the Ni (Figure S3a) and Pd (Figure S3b) cases are more stable by 0.74 and 1.03 eV per unit cell in the configurations they adopt in the crystal, whilst similarly the Pt case (Figure S3c) is more stable by 0.61 eV per unit cell also in the configuration evinced by the experiment.

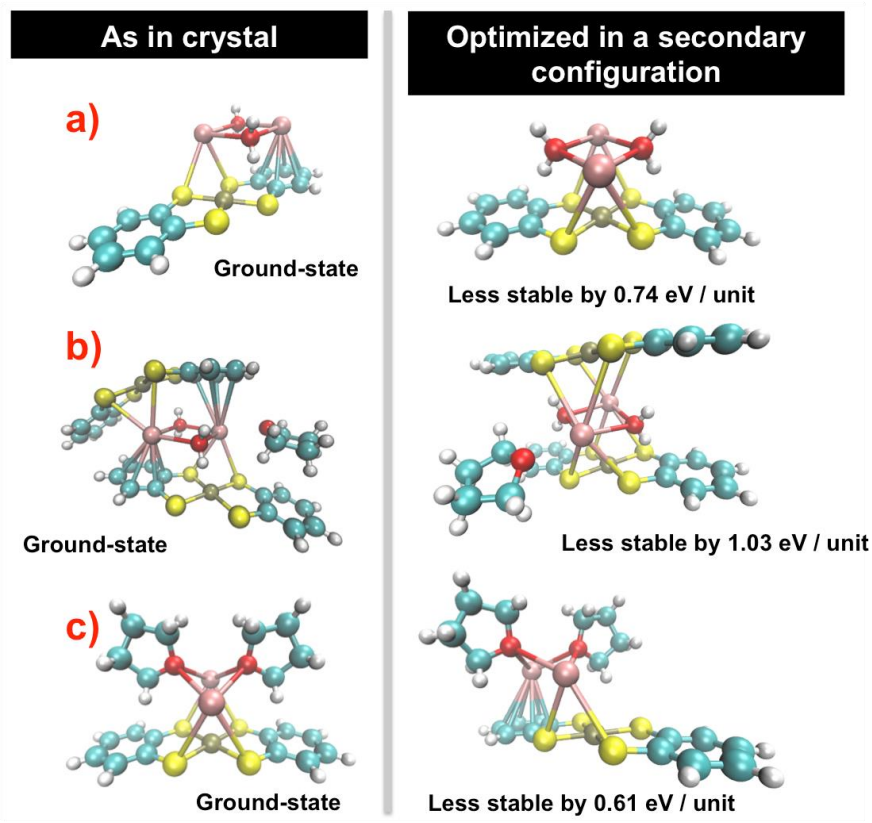

Figure S3. Pictorial view of the building block geometries within the Ni (a), Pd (b) and Pt (c) compounds in two different configurations each: (left) as they form in crystal; and (right) in an optimized "forced" alternative configuration. Ground-state and relative total energy w.r.t. the ground-state are shown for each configuration.

In conclusion, DFT-based calculations justify by both electronic and energetic considerations the packing configurations adopted by the building blocks within the different Ni, Pd and Pt crystals. A priori one could think that all the configurations should be equivalent in all of them, since Ni, Pd and Pt belong to the same periodic-table group with same number of *d* electrons. Nevertheless, slight differences in atomic size and orbital distribution in the metal atoms are sufficient to form essentially different orbital hybridizations and change the packing arrangement from one compound to another.

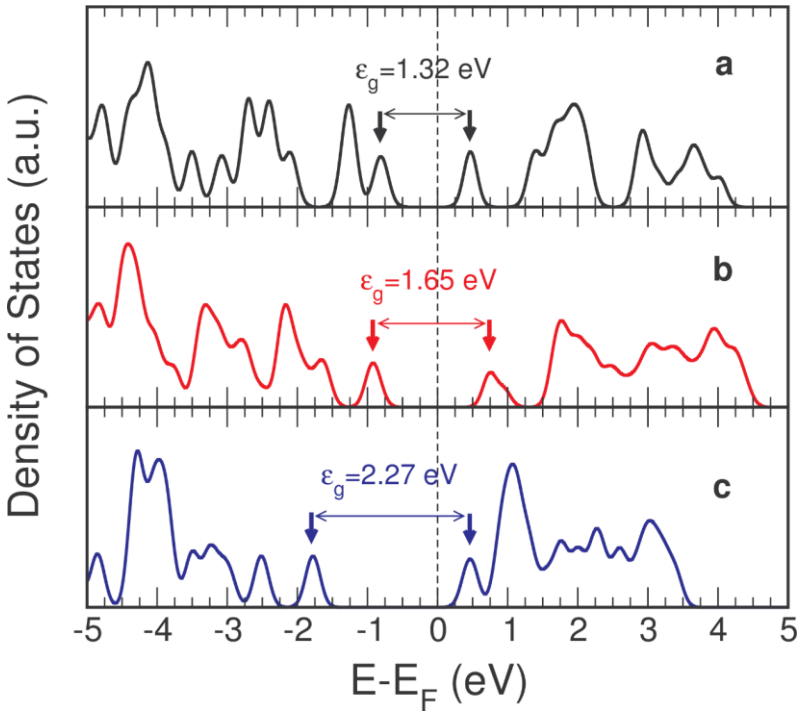

Figure S4. Computed density of states (in a.u.) as a function of the energy (in eV; referred to the Fermi energy) for the $[M(SC_6H_4S)_2]$ M= Ni (a), Pd (b) and Pt (c) compounds. Energy gaps between the valence and conduction bands are shown in each subpanel.

S2. Physical Properties

Magnetic Properties. Magnetic susceptibility measurements performed with the crystals immersed in their mother liquor to avoid contact with air show that compounds **1**-**3** are diamagnetic, with very low room temperature $\chi_m T$ values in the range 0.004-0.025 cm^3 $K\ mol^{-1}$, corresponding to *ca*. 1-6 % of the contribution of one electron. The diamagnetism observed in these compounds is the expected one for square planar Ni(II), Pd(II) and Pt(II) complexes with a d^8 configuration.

Electrical Properties. DC electrical conductivity measurements performed on samples **1**-**3** show that all the samples are semiconductors with room temperature conductivities in the range 6×10^{-9} to 6×10^{-7} Scm^{-1} and activation energies in the range *ca*. 710-740 meV (Table S1). All the crystals where initially cooled from 300 to 200-250 K until the resistance of the sample reached the detection limit of our equipment (5×10^{11} W) (Figure S5). This initial cooling shows a very rapid increase of the resistivity as the temperature is lowered with very high activation energies in the range *ca*. 2000-3000 meV except in compound **3**, where the increases are softer with activation energies of *ca*. 700-800 meV (Figure S6). In a second scan the samples were heated up to 400 K. In **1** and **2** the resistivity of the heating scan is higher than the one observed in the initial cooling scan, suggesting that the rapid increase of the resistivity during the initial cooling scan was due to a progressive irreversible degradation of the sample when it is submitted to low pressure (probably due to a loss of crystallinity as a result of some solvent lost). This initial degradation is not observed in **3** and, accordingly, the first heating scan in similar to the first cooling scan. During the first heating scan all the samples show semiconducting behaviors with very similar activation energies in the range 710-775 meV (Table S1) and reach resistivity minima at *ca*. 310-350 K (Figure S5). On further heating, all the samples show resistivity increases reaching maxima at *ca*. 360-380 K to decrease again until 400 K. When the crystals are cooled from 400 K to 300 K they all show higher resistivity values and higher activation energies (in the range 870-1410 meV (Table S1) than those observed during the heating scan, indicating that the thermal degradation during the first heating scan is irreversible.

Compound **3** shows a larger thermal stability and requires up to three thermal cycles in the temperature range 200-400 K to completely degrade (Figure S5). Thus, during the

first thermal cycle the activation energy of **3** only increased from 740 to 870 meV, but after three cycles the activation energy was 1540 meV (Figure S6). Note that this sample was also more stable at room temperature and did not show the initial degradation when submitted to vacuum. It seems that sample **3** is more stable probably due to the bigger thermal stability of the double thf bridge connecting the K^+ ions when compared with the double H_2O bridges observed in **1** and **2**.

In all cases the similar electrical conductivities and activation energies can be attributed to the presence of similar pathways for the electron delocalization implying the M-dithiolene units, the K-S and K-O interactions. The complexity of the possible delocalization pathways and the similarity of the conductivity values observed in the five samples, precludes any correlation between the structure and the electrical conductivity. Furthermore, as indicated above, we have observed that most crystals show a rapid degradation when they are submitted to low pressure and, therefore, the measured value might be lower that the real ones.

Table S1. Room temperature electrical conductivities and activation energies (E_a) for compounds **1**-**3**.

Compound	$\sigma_{300\ K}$ (S/cm)	E_a[a] (meV)	E_a[b] (meV)
1	6×10^{-7}	720	1120
2	1×10^{-8}	710	1410
3	6×10^{-9}	740	870/1540[c]

[a]before heating at 400 K; [b]after heating at 400 K; [c]after three thermal cycles.

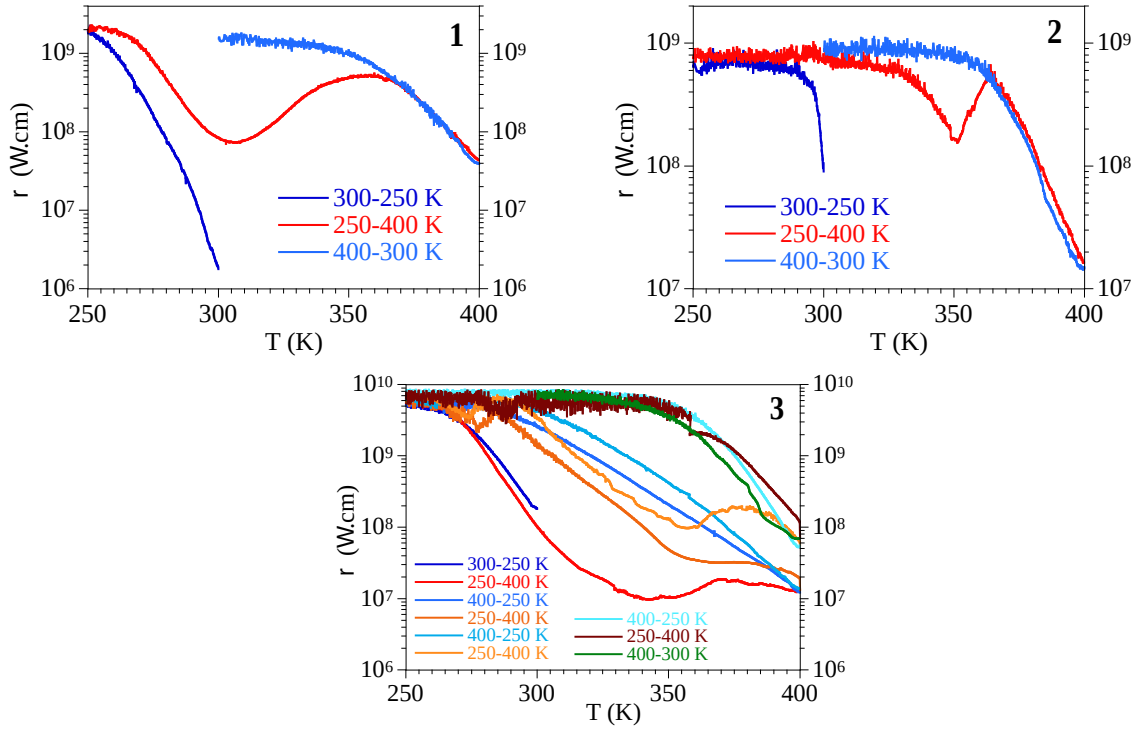

Figure S5. Thermal variation of the electrical resistivity of samples **1-3** during different cooling and heating scans.

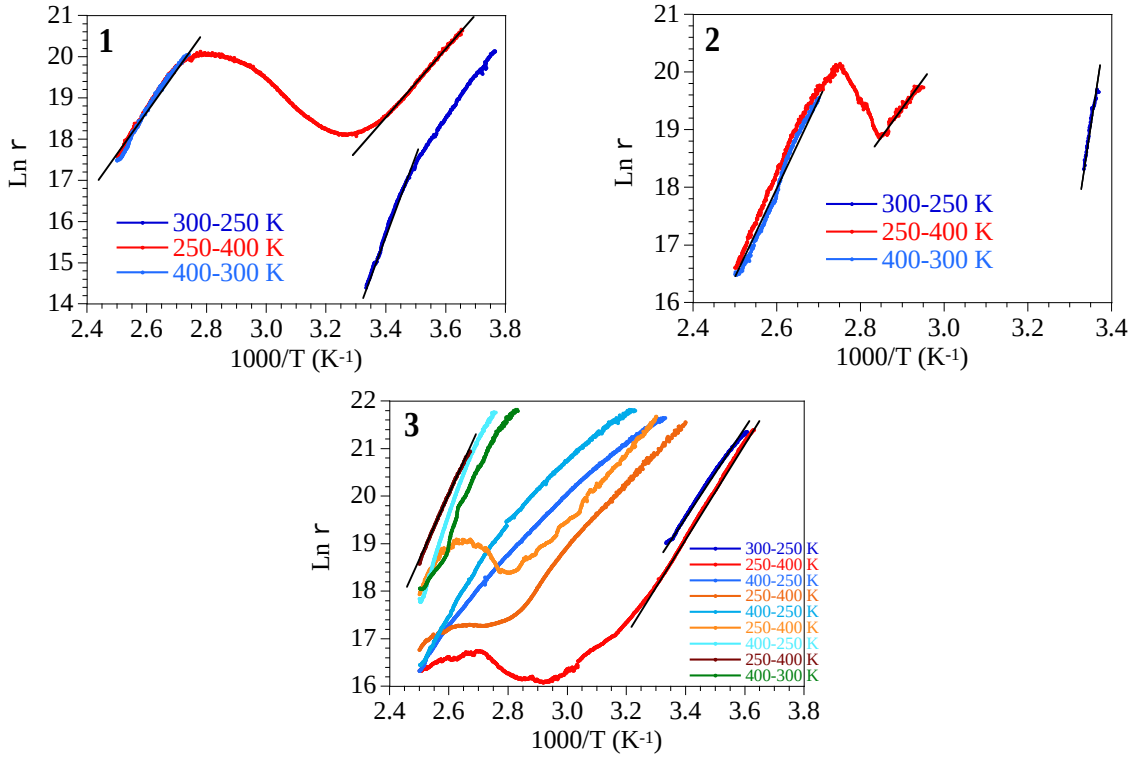

Figure S6. Arrhenius plots of compounds **1-3** during different cooling and heating scans. Solid lines are the fits to the Arrhenius equation.

References

[1] G. A. Bain and J. F. Berry, *J. Chem. Educ.*, 2008, **85**, 532-536.

[2] L. J. Farrugia, *J. Appl. Cryst.*, 2012, **45**, 849-854.

[3] G. M. Sheldrick, *Acta Crystallogr.*, 2008, **A64**, 112-122.

[4] G. M. Sheldrick, *Acta Crystallogr.*, 2015, **C71**, 3-8.

[5] G. M. Sheldrick, *Acta Crystallogr.*, 2015, **A71**, 3-8.

[6] P. W. Ayers and R. G. Parr, *J. Am. Chem. Soc.*, 2000, **122**, 2010-2018.

[7] P. W. Ayers, R. C. Morrison and R. K. Roy, *J. Chem. Phys.*, 2002, **116**, 8731-8744.

[8] *Gaussian 09, Revision **E.01**, Frisch, M. J.; et al., Gaussian, Inc., Wallingford CT (2009).*

[9] H. Wang, S. M. Butorin, A. T. Young and J. Guo, *J. Phys. Chem. C*, 2013, **117**, 24767-24772 .

[10] P. Giannozzi, S. Baroni, N. Bonini, M. Calandra, R. Car, C. Cavazzoni, D. Ceresoli, G. L. Chiarotti, M. Cococcioni, I. Dabo, A. D. Corso, S. de Gironcoli, S. Fabris, G. Fratesi, R. Gebauer, U. Gerstmann, C. Gougoussis, A. Kokalj, M. Lazzeri, L. Martin-Samos, N. Marzari, F. Mauri, R. Mazzarello, S. Paolini, A. Pasquarello, L. Paulatto, C. Sbraccia, S. Scandolo, G. Sclauzero, A. P. Seitsonen, A. Smogunov, P. Umari and R. M. Wentzcovitch, *J. Phys. Condens. Matter*, 2009, **21**, 395502-395521.

[11] J. P. Perdew, K. Burke and M. Ernzerhof, *Phys. Rev. Lett.*, 1997, **78**, 1396-1396.

[12] A. M. Rappe, K. M. Rabe, E. Kaxiras and J. D. Joannopoulos, *Phys. Rev. B*, 1990, **41**, 1227-1230.

[13] H. J. Monkhorst and J. D. Pack, *Phys. Rev. B*, 1976, **13**, 5188-5192.

[14] V. Barone, M. Casarin, D. Forrer, M. Pavone, M. Sambi and A. Vittadini, *J. Comput. Chem.*, 2009, **30**, 934-939.

[15] S. Grimme, *J. Comput. Chem.*, 2006, **27**, 1787-1799.